

Measurement of graphite tight-binding parameters using high field magneto-reflectance

L.-C. Tung,^{1,2} P. Cadden-Zimansky,^{1,3} J. Qi,¹ Z. Jiang,⁴ and D. Smirnov¹

¹*National High Magnetic Field Laboratory, Tallahassee, Florida 32310*

²*Department of Physics and Astrophysics, University of North Dakota, Grand Forks, North Dakota 58202*

³*Department of Physics, Columbia University, New York, New York 10027*

⁴*School of Physics, Georgia Institute of Technology, Atlanta, Georgia 30332*

(Dated: July 12, 2018; Received textdate; Revised textdate; Accepted textdate; Published textdate)

Magnetic subbands of graphite have been investigated by magneto-infrared reflectance spectroscopy at 4K in fields up to 31T. Both Schrödinger-like (K-point) and Dirac-like (H-point) Landau level transitions have been observed, and their magnetic field dispersion are analyzed by a newly-derived limiting case of the Slonczewski-Weiss-McClure model. The values of the band parameters are evaluated without using sophisticated conductivity peak lineshape analysis. In this work, several less-explored band parameters are determined from the experimental results and they are known to result in electron-hole asymmetry and the opening of an energy gap between the electron and hole bands in multilayer and bilayer graphene systems.

The tight-binding model of graphite's band structure, first calculated by Wallace[1] and later extended by Slonczewski, Weiss,[2] and McClure[3], has enjoyed a renaissance in recent years due to its successful application in understanding many properties of single and few-layer graphene.[4, 5] The model, known as Slonczewski-Weiss-McClure (SWMc) band theory, rests on seven tight binding parameters, γ_0 to γ_5 and Δ , characterizing interactions between near neighbor atoms in the lattice. The physical representations and estimated values of these parameters have been illustrated and organized by Dresselhaus *et al.*[6] and Zhang *et al.*[7]. While the SWMc model has been used in understanding graphitic materials for the last 60 years[6–14], the values of less-explored band parameters (γ_4 , γ_5 and Δ) remain uncertain. As these parameters may play an expanded role in interpreting observed asymmetries in the electronics of graphene, there is an increased incentive to accurately measure them.

Infrared (IR) (magneto)-spectroscopy is a powerful tool in resolving energies in the band structure of graphitic materials, and has already been employed to study the unique electronic states of massless Dirac-like fermion in monolayer graphene[15–17], massive chiral fermions in bilayer graphene[7, 22–24], and rich spectral features in graphite[6, 12, 13, 18–21], where effects attributed to both massless holes and massive electrons have been seen. The results in graphite have been modeled by assuming that its band structure is a combination of a monolayer model, where the holes at the Brillouin zone H-point behave like massless fermions, and an effective bilayer model (EBM)[19–21], where the electrons at the K-point behave like massive fermions with an adjusted coupling constant between layers. However, the EBM ignores the band parameters governing the interlayer hoppings between unstacked and stacked/unstacked sublattices (γ_3 , γ_4), next-nearest interlayer hoppings (γ_2 , γ_5), and the on-site energy difference between the stacked and unstacked sublattices (Δ). Excluding these

parameters removes the possibility of electron-hole ($e-h$) asymmetry, which has been observed to be significant in bilayer graphene and graphite.[7, 18, 21, 22, 24]

The interlayer hoppings can also drastically change the band structure near the charge neutrality point (CNP), i.e. the point where the electron and hole bands touch, and lift the degeneracy of the doubly degenerate $e-h$ mixed Landau level, (LL-1) and (LL0). Here, we use the level indexing notation of ref. [11]. The (LL-1) and (LL0) refer to the two LLs near the CNP, and the term, $hn-em$, refers to a transition from the n -th hole LL to the m -th electron LL. The splitting of the two $e-h$ mixed LLs was observed recently by Li *et al.*[18], and the transition between these two states exhibits a potential 3D to 1D crossover due to graphite's anisotropic properties.

In this communication, we use IR spectroscopy to measure the magnetic-field dispersion of graphite's LLs and fit our measurements to a newly-derived limit of the SWMc model that includes higher-order band parameters. The intense magnetic fields applied distinguish the two $e-h$ mixed LLs and split of the $e-h$ symmetry of several interband transitions. These lifted degeneracies are accounted for by our modified SWMc model, and values for the set of band parameters are found consistent with those previously reported.[6, 7]

Our measurement set-up uses Kish graphite flakes stabilized on the Scotch tape and placed in a cryostat held at 4K subjected to magnetic fields of up to 31T. IR reflectance spectra are measured by a Fourier transform IR interferometer using light pipe optics. The reflectance is then normalized by taking the ratio of the sample spectra to that of a gold mirror. The acquired reflectance spectra are modeled by Drude-Lorentz functions using RefFit. Sharp or minute features attributable to noise were smoothed prior to modeling. To show the quality of the modeling, the smoothed reflectance spectra are plotted in Fig. 1 overlaid with the original spectra at every other Tesla. Further analysis reveals that the observed

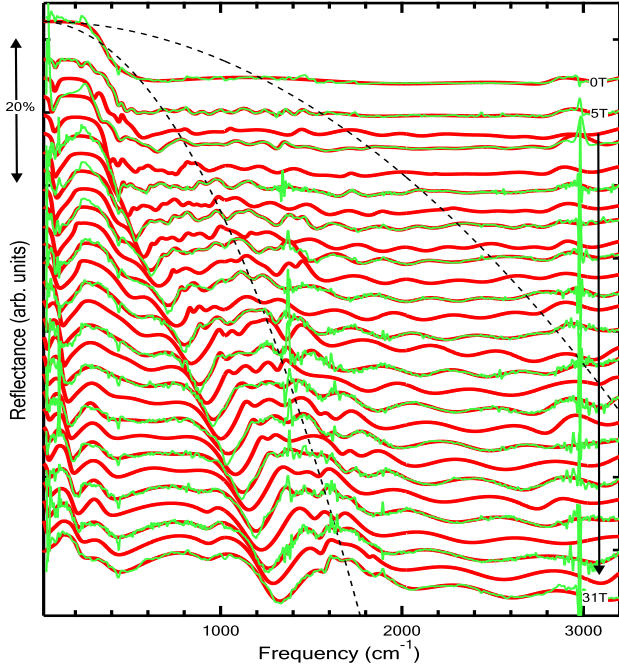


FIG. 1: Reflectance spectra of graphite: The spectra are vertically shifted for clarity. The smoothed (original) spectra are shown in thick red (thin green) lines. Two dashed lines are used as guides for spectral features following \sqrt{B} -dependence.

oscillatory spectral features are attached to the K- and H-point transitions, exhibiting linear in B and \sqrt{B} -dependence, respectively. The features resulting from $e-h$ mixed LLs are located at low frequencies, while $e-h$ asymmetry results in splitting in several of the interband transitions at high frequencies.

The dynamic conductivity, shown in Fig 2, can be calculated from the modeling of Fig. 1, and exhibits a series of magnetic-field dependent conductivity peaks. The overall profile of the dynamic conductivity is consistent with a recent theoretical calculation in the presence of a moderate magnetic field[25], and most K-point transitions show sizeable deviation from the linear dependence. The two lowest-energy modes, resulting from the (LL-1)-(LL0) and (LL0)-e1 transitions, are displayed in Fig. 2 (a). It is obvious that magnetic-field dispersion of the (LL0)-e1 transition is not linear, instead exhibiting an interesting crossover from linear (low-field) to nonlinear (high-field) dependence.

Graphite has been shown to exhibit a universal conductance $G_0 = e^2/4\hbar$ for photon energies between 0.1 to 0.6eV at zero magnetic field.[26] ($1\text{eV} = 8065\text{cm}^{-1}$) The sheet conductance of our sample, calculated using $G(\omega) = c_0\sigma(\omega)$ with interlayer distance $c_0 = 3.35\text{\AA}$, is shown in the inset of Fig. 2 (b). The calculated value is found larger than $G_0 = e^2/4\hbar$, but closer to $4e^2/h$. Accounting for this discrepancy, one should note that the conductivity is not calculated from a true Kramer-Kronig

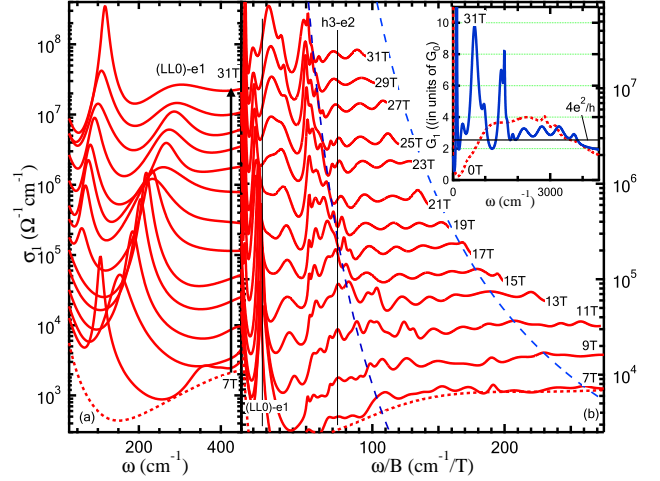


FIG. 2: Real part (σ_1) of the dynamic conductivity: The curves are shifted vertically for clarity. For comparison, σ_1 at $B = 0\text{T}$ is shown in a dotted line. To help the readers locating the modes in (b), two vertical lines mark the peaks associated with the (LL0)-e1 and h3-e2 transitions. Two guide lines similar to Fig. 1 follow the H-point transitions. Inset: Sheet conductance per graphene layer at $B = 0\text{T}$ and 31T are shown in units of $G_0 = e^2/4\hbar$.

transformation, but a result of modeling the reflectance spectra using finite numbers of Drude-Lorentz functions. As one cannot precisely assign Lorentz modes outside the measurement range, the optical weight for the modes located within the measurement range tends to be overestimated. Moreover, the incident angle and the misalignment (between the sample and the gold reference) can also affect the result. On the other hand, the universal conductance is dependent on the short-range disorder, "ripples" in graphene's atomic structure and the presence of charged impurities[27, 28], all of which are likely to be present in Kish graphite. The focus of this work is the magnetic-field dispersion of the LLs, which are not impacted by the frequency-independent universal conductance.

Mode energies extracted from the conductivity peaks of Fig. 2 are plotted in Fig. 3, with modes following \sqrt{B} -dependence shown in (a) and those following linear dependence shown in (b). The (LL0)-e1 transition follows linear dependence below 12T, but \sqrt{B} -dependence at higher fields, and thus is plotted in both panels. Anomalies in mode energies can be found around the characteristic phonon energies of graphite[29, 30], particularly along several LL transitions (H: -1 to 0, K: (LL0)-e2, h1-e2), which will be further investigated elsewhere.

In order to invoke the SWMc model, we start with the theoretical observation that the LL structures for $\gamma_3 = 0$ and $\gamma_3 \neq 0$ are similar at high fields[11, 21], and so set $\gamma_3 \equiv 0$, which ignores the trigonal warping in the band structure. The energy of the magnetic subbands can then

be obtained using the following self-consistent Eq.[9],

$$(n + \frac{1}{2})\tilde{E}^2 = \varepsilon \left[\frac{\varepsilon(1 + \nu^2)}{(1 - \nu^2)^2} + \frac{\delta\omega}{(\omega^2 - \delta\omega^2)} \right] \quad (1)$$

$$\pm \sqrt{\left[\varepsilon \left(\frac{2\varepsilon\nu}{(1 - \nu^2)^2} - \frac{\omega}{(\omega^2 - \delta\omega^2)} \right) \right]^2 + \left(\frac{\tilde{E}^2}{2} \right)^2},$$

where integer n is the LL index, $\varepsilon = E - E_3$, $\tilde{E}^2 = \tilde{c}^2 2e\hbar B = qB$ with $\tilde{c} = \frac{\sqrt{3}a_0\gamma_0}{2\hbar}$, $\nu = \frac{\gamma_4\Gamma}{\gamma_0}$ with $\Gamma = 2 \cos(\frac{c_0 k_z}{2})$, $\omega = \frac{1}{2} \left[\frac{(1-\nu)^2}{E_1 - E_3} - \frac{(1+\nu)^2}{E_2 - E_3} \right]$ and $\delta\omega = \frac{1}{2} \left[\frac{(1-\nu)^2}{E_1 - E_3} + \frac{(1+\nu)^2}{E_2 - E_3} \right]$, in which c_0 and a_0 are lattice parameters. In SWMc model, E_1 , E_2 , and E_3 can be represented as[9],

$$E_{1,2} = \Delta \pm \gamma_1\Gamma + \frac{1}{2}\gamma_5\Gamma^2 \text{ and } E_3 = \frac{1}{2}\gamma_2\Gamma^2. \quad (2)$$

At H-point, where $\Gamma = 0$, the levels are[9],

$$E = \frac{\Delta}{2} \pm \sqrt{\left(\frac{\Delta}{2}\right)^2 + nqB}. \quad (3)$$

Using the modes following \sqrt{B} -dependence, we find that the data agree well with the Fermi velocity $\tilde{c} = 1.03 \times 10^6$ m/s ($\gamma_0 = 3.18\text{eV}$) and assign the two highest energy modes to the $n = -1$ to $n = 0$ and $n = -1(-2)$ to $n = 2(1)$ transitions. To see if the parameter Δ is finite, the energy $E_{-1,0}$ for the $n = -1$ to $n = 0$ transition is scaled by a factor of $1 + \sqrt{2}$, and plotted in a dotted line in Fig. 3 (a). If Δ is finite, the scaled energy $(1 + \sqrt{2})E_{-1,0}$ would be larger than the interband transition energy $E_{-1,2}$. [15] From the difference, $|\Delta|$ is estimated to be 60 cm^{-1} .

For K-point transitions, the levels follows a linear in B dependence when \tilde{E} is small, and can be written as[9]

$$\varepsilon_{e,h} = \left[\pm \sqrt{n(n+1)\omega^2 + \frac{1}{4}\delta\omega^2} - (n + \frac{1}{2})\delta\omega \right] qB, \quad (4)$$

in which ω determines the energy separation between the LLs and $\delta\omega$ results in the $e - h$ asymmetry. It is clear from the data that most K-point modes are not linear at high fields. Though having a nonlinear magnetic field dispersion, the EBM[20, 21] ignores the $e - h$ asymmetry; an effect one cannot sufficiently account for by using two different Fermi velocities[21], since the correction is apparently dependent on the LL index n . On the other hand, It worths noting that the EBM[20, 21] and the bilayer model[31] ($\Gamma = 1$) can be obtained by approximating the self-consistent Eq. (1) of the SWMc model as,

$$\varepsilon^2 \cong \frac{2n+1}{2}\tilde{E}^2 + \frac{1}{2}\frac{1}{\omega^2} - \frac{1}{2}\sqrt{\frac{1}{\omega^4} + 4\frac{\varepsilon^2}{\omega^2} + \tilde{E}^4}. \quad (5)$$

and use a trial $\varepsilon^2 = \frac{2n+1}{2}\tilde{E}^2$ on the right-hand side.

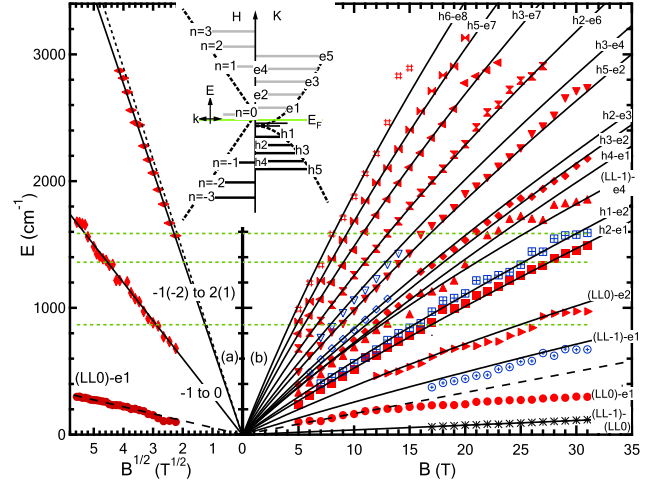


FIG. 3: Transition energies as a function of magnetic field: Three green dotted horizontal lines mark the characteristic phonon energies in graphite. Black solid lines are fittings using Eq. (3) for panel (a) and Eq. (6) for panel (b). The purpose of the dashed lines is explained in the text. Inset: Schematic energy diagram at the H- and K-point.

To derive a working formula to account for the non-linear magnetic field dependence of K-point transitions at high fields and with $e - h$ asymmetry, it is instructive to re-examine the Eq. (1). If the term $(\frac{\tilde{E}^2}{2})^2$ is neglected, Eq. (1) becomes a simple quadratic equation. Using graphite's band parameters, the term $(\frac{\tilde{E}^2}{2})^2$ can be neglected when $\frac{\varepsilon}{B} \gg 8 \text{ cm}^{-1}/\text{T}$, a condition can be met for any $n \geq 1$ levels. With this approximation, the magnetic levels can then be calculated to be

$$\varepsilon_{e,h} = \frac{(1 \pm \nu)^2}{2} \left[\mp \frac{1}{\omega \mp \delta\omega} \pm \sqrt{\left(\frac{1}{\omega \mp \delta\omega} \right)^2 + \frac{2(2n+1)}{(1 \pm \nu)^2} qB} \right]. \quad (6)$$

Interestingly, when $\nu = 0$, Eq. (6) can be written as

$$\varepsilon_{e,h} = \pm \sqrt{(m_{e,h}\tilde{c}^2)^2 + 2n'\hbar\omega_c \cdot m_{e,h}\tilde{c}^2 - m_{e,h}\tilde{c}^2}, \quad (7)$$

where $m_{e,h} \equiv \frac{1}{\tilde{c}^2} \frac{1}{2(\omega \mp \delta\omega)}$, $n' = (n+1/2)$, and ω_c is the cyclotron frequency. The first term in Eq. (7) agrees with a solution of the Dirac equation in a magnetic field except for that the value of n' was supposed to be integers.[32] Eq. (7) mimics the relativistic kinetic energy of a massive particle. Using this analogy, the effect of ν may be regarded as a Doppler effect, which causes blueshifts (redshifts) to electrons (holes).

In analyzing the $e - h$ asymmetry, potential assignments for the higher-energy modes can be arbitrary (due to the large number of possible combinations), thus we use only the lower-energy modes to determine the band parameters. Good agreement with the data can be

achieved using $\omega q = 14.5 \text{ cm}^{-1}/\text{T}$, $\delta\omega q = -3.4 \text{ cm}^{-1}/\text{T}$ and $\nu = 0.05$. The calculated transition energies are shown in solid lines in Fig. 3 (b) and the higher-energy modes are assigned to the transitions that best describe the magnetic-field dispersion of the transition energies. Near the K-point, i.e. $\gamma_1\Gamma \gg \Delta + \frac{1}{2}\gamma_5\Gamma^2 - \frac{1}{2}\gamma_2\Gamma^2$, the fitting parameters, ω and $\delta\omega$, are related to the band parameters as

$$\omega \sim \frac{1}{\gamma_1\Gamma}; \quad \delta\omega \sim -\frac{\frac{\Delta}{\Gamma^2} + 2\gamma_4\frac{\gamma_1}{\gamma_0} + \frac{1}{2}\gamma_5 - \frac{1}{2}\gamma_2}{\gamma_1^2}. \quad (8)$$

From the values of fitting parameters, we extract $\gamma_1 = 0.38\text{eV}$, $\gamma_4 = 0.08\text{eV}$ and $-\gamma_2 + \gamma_5 = 0.048\text{eV}$. It is generally agreed[6, 7] that $\gamma_2 = -0.02\text{eV}$, so γ_5 is estimated to be 0.028eV .

For the (LL-1) and (LL0) levels (i.e. $n = 0$), one can solve the cubic Eq. in Ref. [10] to find

$$\varepsilon = 0 \text{ and } \varepsilon \sim -\delta\omega q B, \quad (9)$$

respectively. Since the (LL0) level will be partially occupied by electrons, the transition between the (LL-1) and (LL0) levels are made by those electrons away from the K-point. The parameter $\delta\omega(k_z \sim k_F)q$ is found to be $-3.7\text{cm}^{-1}/\text{T}$, which is slightly larger than $\delta\omega(k_z = 0)q = -3.4\text{cm}^{-1}/\text{T}$; therefore, the sublattice energy difference Δ is likely to be positive.

The (LL0)-e1 transition exhibits an unusual crossover. At lower fields, its energy agrees with the prediction of the linear SWMc model with a slope of $17\text{cm}^{-1}/\text{T}$. (dashed line in Fig. 3 (b)) At higher fields, the peak broadens quickly with increasing magnetic field, and the magnetic-field dispersion becomes Dirac-like with a slope of $54\text{cm}^{-1}/\text{T}^{1/2}$. (dashed line in Fig. 3 (a)) A similar behavior has been reported previously[18], where the (LL0)-e1 mode has a larger slope for $B \leq 8.5\text{T}$, but a smaller slope for $B \geq 8.5\text{T}$. In addition, we find that $E_{(LL-1)-(LL0)} + E_{(LL0)-e1} < E_{(LL-1)-e1}$, a discrepancy that cannot be accounted for by simple pictures assuming LLs are independent with each other. Except for the (LL0)-e1 transition, all other transitions are well described by the modified SWMc model (Eq. (6)), so the underlying mechanism for this anomaly is specific to the (LL0) level. Anomalous phenomena have been observed pertaining to this level, and it has been conjectured that a charge density wave[33–35] has an effect specific to it, though it should be noted that these anomalies were found at lower temperatures and at higher fields.

In summary, magnetic subbands in Kish graphite are investigated using magneto-infrared reflectance spectroscopy up to 31T. The high magnetic field distinguishes the two $e-h$ mixing LLs near the CNP and the splitting of the interband transitions. We propose a new limit of the SWMc model to describe the K-point transitions and

use it to estimate the values of the band parameters,

$$\begin{aligned} \gamma_0 &= 3.18\text{eV}, \gamma_1 = 0.38\text{eV}, \gamma_2 = -0.02\text{eV}, \gamma_3 \equiv 0, \\ \gamma_4 &= 0.08\text{eV}, \gamma_5 = 0.028\text{eV}, \text{ and } |\Delta| = 0.008\text{eV}. \end{aligned}$$

This work was supported by the DOE (DE-FG02-07ER46451) and the NSF (DMR-0820382). The IR measurement was carried out at the National High Magnetic Field Laboratory, which is supported by NSF Cooperative Agreement No. DMR-0654118, by the State of Florida, and by the DOE.

-
- [1] P. R. Wallace, Phys. Rev. **71**, 622 (1947)
 - [2] J. C. Slonczewski and P. R. Weiss, Phys. Rev. **109**, 272 (1958)
 - [3] J. W. McClure, Phys. Rev. **108**, 612 (1957)
 - [4] K. S. Novoselov *et al.*, Science **306**, 666 (2004)
 - [5] For a review, see A. H. Castro Neto, F. Guinea, N. M. Peres, K. S. Novoselov and A. K. Geim, Rev. Mod. Phys. **81**, 109 (2009)
 - [6] For a review, see M. S. Dresselhaus and G. Dresselhaus, Adv. Phys. **30**, 139 (1981)
 - [7] L. M. Zhang *et al.*, Phys. Rev. B **78**, 235408 (2008)
 - [8] N. B. Brandt, S. M. Chudinov, and Y. G. Ponomarev, *Semimetals I: Graphite and its Compounds* (North-Holland, Amsterdam, 1988).
 - [9] J. W. McClure, Phys. Rev. **119**, 606 (1960)
 - [10] M. Inoue, J. Phys. Soc Jpn. **17**, 808 (1962)
 - [11] K. Nakao, J. Phys. Soc. Jpn **40**, 761 (1976)
 - [12] W. W. Toy, M. S. Dresselhaus and G. Dresselhaus, Phys. Rev. B **15**, 4077 (1977)
 - [13] R. E. Doezema, W. R. Datars, H. Schaber and A. Van Schyndel, Phys. Rev. B **19**, 4224 (1979)
 - [14] S. B. Hubbard, T. J. Kershaw, A. Usher, A. K. Savchenko, and A. Shtyov, Phys. Rev. B **83**, 035122 (2011)
 - [15] Z. Jiang *et al.*, Phys. Rev. Lett. **98**, 197403 (2007)
 - [16] R. S. Deacon, K.-C. Chuang, R. J. Nicholas, K. S. Novoselov, and A. K. Geim, Phys. Rev. B **76**, 081406 (2007)
 - [17] E. A. Henriksen *et al.*, Phys. Rev. Lett. **104**, 067404 (2010)
 - [18] Z. Q. Li *et al.*, Phys. Rev. B **74**, 195404 (2006)
 - [19] M. Orlita *et al.*, Phys. Rev. Lett. **100**, 136403 (2008)
 - [20] M. Orlita *et al.*, Phys. Rev. Lett. **102**, 166401 (2009)
 - [21] K.-C. Chuang, A. M. R. Baker, and R. J. Nicholas, Phys. Rev. B **80**, 161410 (2009)
 - [22] E. A. Henriksen *et al.*, Phys. Rev. Lett. **100**, 087403 (2008)
 - [23] Z. Q. Li *et al.*, Phys. Rev. Lett. **102**, 037403 (2009)
 - [24] A. B. Kuzmenko *et al.*, Phys. Rev. B **79**, 115441 (2009)
 - [25] L. A. Falkovsky, Phys. Rev. B **83**, 081107 (2011)
 - [26] A. B. Kuzmenko, E. van Heumen, F. Carbone, and D. van der Marel, Phys. Rev. Lett. **100**, 117401 (2008)
 - [27] J.-H. Chen *et al.*, Nature Phys. **4**, 377 (2008) and reference therein.
 - [28] S. V. Morozov *et al.*, Phys. Rev. Lett. **100**, 016602 (2008) and reference therein.
 - [29] S. Reich and C. Thomsen, Phil. Trans. R. Soc. Lond. A **362**, 2271 (2004)

- [30] A. C. Ferrari, Solid State Commun. **143**, 47 (2007)
- [31] E. McCann and V. I. Fal'ko, Phys. Rev. Lett. **96**, 086805 (2006)
- [32] A. A. Sokolov and I. M. Ternov, The Relativistic Electron. Moscow: Nauka, 391 (1974)
- [33] D. Yoshioka and H. Fukuyama, J. Phys. Soc. Jpn **50**, 725 (1981);
- [34] Y. Iye *et al.*, Phys. Rev. B **25**, 5478 (1982)
- [35] K. Sugihara, Phys. Rev. B **29**, 6722 (1984)